

THE NARROW GROOVE ANALYSIS REVISITED

Coda H. T. Pan
Engineering Consultant
Millbury, Massachusetts 01527, USA

Luis San Andrés
Mechanical Engineering Department, Texas A&M University,
College Station, Texas 77843-3123, USA

ABSTRACT

The narrow groove analysis (NGA) as pioneered by Whipple [1] is a two-scale formulation with an infinitesimal micro-scale. Its shortcomings include: ambiguity in minimum required number of grooves, implied assumption of local incompressibility, violation of end conditions and omission of local squeeze effect. Alternative numerical computation methods of the finite-element or finite-volume type [2][3] to treat the problem with a finite number of grooves are at best very expensive because good designs tends to require a large number of grooves.

In view that interest in inclined groove gas lubricated devices has intensified [3], a new two-scale formulation is presented here to consider a small but finite micro-scale. Cross-pattern profiles of pressure and induced transverse flux are presented for the entrance condition of a typical thrust bearing with eighteen spiral-grooves.

NOMENCLATURE

C	Nominal bearing clearance
H	h/C
Kn_a	λ_a/h . Knudsen number
P	Subdomain pressure; p/p_0
\bar{P}	Macro-scale pressure
R	Outer radius
α	Groove width fraction; $\Delta\xi_g = 1 - \Delta\xi_l$
β	Angular inclination of groove to radius
η	Groove-wise coordinate
φ	Micro-scale circumferential flux
Φ_ζ	Subdomain radial flux
λ_a	Molecular MFP of gas
Λ	$6\mu\omega(\zeta R/C)^2 (\bar{P}/p_a)$
$\tilde{\Lambda}$	$\Delta\theta\Lambda$
μ	Gas viscosity
θ	Angular coordinate
$\Delta\theta$	Pattern width
ω	Rotation rate
σ_p	Rarefaction flow factor
ξ	$\theta/\Delta\theta$
ζ	Radial coordinate; r/R
Ψ	Macro-scale radial flux

Subscripts

g, l pertaining to groove- or land-subdomain
 E, I pertaining to groove-end or inner radius

THE FNGA STRATEGY

NGA comprises a macro-scale part that discretizes the bearing planform into an $M \times N$ grid and a micro-scale analysis that treats the cross-pattern pressure profile P and transverse flux Φ_ζ . Spanwise averaging of P and Φ_ζ yields the macro-scale counterparts \bar{P} and Ψ . Micro-scale analysis involves solving the gas film flux law across span $\Delta\theta = 2\pi n$. For $n \rightarrow \infty$, $\Delta\theta$ becomes nil; this is infinitesimal narrow groove analysis (INGA). For a finite n , $\Delta\theta$ is also finite. The finite narrow groove analysis (FNGA) constructs the cross-pattern solution with a concatenated integral that features local compressibility. The cross-pattern solution of either INGA or FNGA so obtained is an interior solution as the micro-scale pressure profile is defective in violating the isobaric ambient boundary condition and the condition of radial pressure continuity across the groove end. Both defects can be corrected upon appropriate coupling of micro- and macro-scale computations.

MICRO-SCALE ANALYSIS

Allowing for rarefaction with fully diffused wall-molecular interaction [5], the cross-pattern flux law is

$$\varphi = PH - \sigma_p \tilde{\Lambda}^{-1} PH^3 (\partial P / \partial \xi) \quad (1)$$

CROSS-PATTERN SOLUTION

Equation (1) satisfies the integral formula [6] separately in the groove- and land-subdomains:

$$\int_{\text{start}}^{\text{finish}} \frac{\sigma_p PH d(PH)}{[\tilde{\Lambda} + \sigma_p (dH/d\xi)(PH)](PH) - \varphi} = \int_{\text{start}}^{\text{finish}} \frac{d\xi}{H}$$

σ_p is a function of $Kn_a/(PH)$; it is linearly interpolated in the P -space as a concatenation approximation, making possible the closed form integration of the left-hand side. Upon assigning end-values of P in the respective subdomain, φ is found by iterative computation. Substituting φ back into the indefinite form of Equation (1), $P(\xi)$ can be determined. Continuity across fore- and aft-steps of the groove results in distinct values of $\partial P / \partial \eta$ at the two steps. Within each subdomain $\partial P / \partial \eta$ is found by solving the η -derivative of Equation (1) by numerical quadrature during the process of constructing $P(\xi)$. In turn, it combines with $\partial P / \partial \xi$ to form $\partial P / \partial \zeta$ for calculation of subdomain transverse fluxes Φ_ζ . Cross-pattern integration of (P, Φ_ζ) result in their macro-scale counterparts (\bar{P}, Ψ) .

FNGA distinguishes itself from INGA in bringing out the curvature in $P(\xi)$ and a nonuniform micro-scale radial flux.

GLOBAL SOLUTION WITH END DEFECTS

Postulating that end effects would be dispersed spatially with little influence on \bar{P} , a first order global solution can be computed by requiring global invariance of Ψ over the whole bearing plan form.

SIGNIFICANCE OF BEARING SIZE

FNGA results of a thrust bearing will be presented for a bearing planform drawn in actual proportions as illustrated in Fig. 1. Operating speed up to 100,000 rpm is of immediate interest.

FNGA allows for size effect in terms of $Kn_{aC} = \lambda_a/C$. Assuming the common practice of $C/R \approx 10^{-3}$ is followed, Kn_{aC} would be 0.0705 for 2 mm OD bearing; a moderate level of rarefaction effect is expected.

Rotation rate of 100,000 rpm would render $\Lambda = 12.15$ with $\tilde{\Lambda} = 4.243$ for eighteen grooves. Combinations of $Kn_{aC} = (0, 0.0705)$ and $\Lambda = 12.15$ will be used to compute illustrative results using plan form parameters ($\alpha = 0.60, \beta = 72^\circ, \delta/C = 2.0$).

RESULTS

The gas film in the grooved sub-domain functions as a compressor with internal leakage through the land sub-domain and delivers a process flow load across the annular seal region beyond the groove ends. **FNGA** examines the effects of Λ and Kn_{aC} on the performance parameters of the compressor, as represented by its pressurization capacity, at the delivered flow rate.

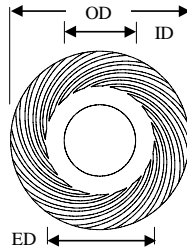


Fig. 1 Typical thrust bearing

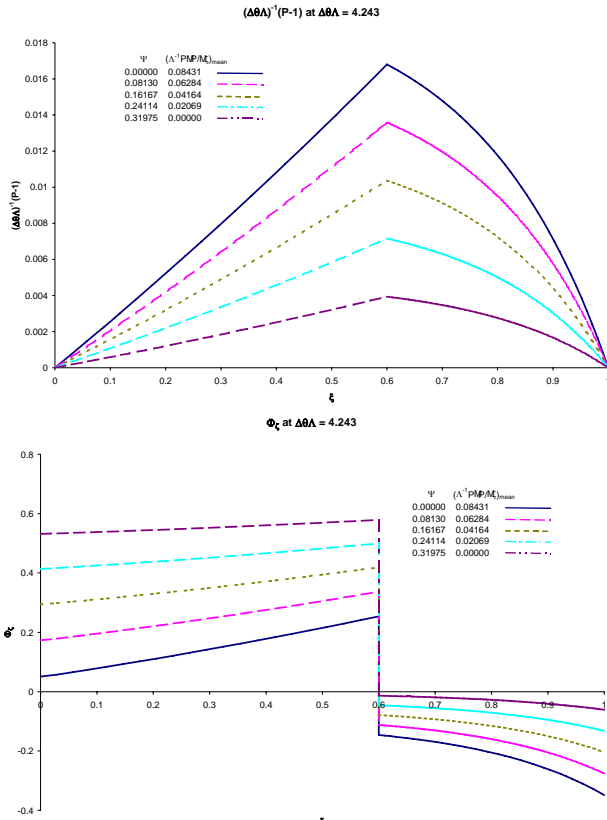


Fig. 2 Profiles computed with FNGA

“Precise” micro-scale computation is the backbone of **FNGA**. Of primary importance are the cross pattern profile P and the induced radial flux Φ_c . They are derived from the solution of Equation (1) and the conditions of flux- and pressure-continuity along the groove sides. Due to the transcendental character of the governing equations, micro-scale computation is performed with an assigned cross-pattern pressure height, $\Delta P/\tilde{\Lambda}$; yielding $P, \Phi_c, (\Lambda^{-1} P \partial P/\partial \zeta)_{\text{mean}}$ and Ψ . In common applications, $\Delta P/\tilde{\Lambda}$ of interest is bracketed between the null condition of Ψ and that of $(\Lambda^{-1} P \partial P/\partial \zeta)_{\text{mean}}$, which are found by iterative computation. For illustration, profiles of P and Φ_c , as computed for five values of $\Delta P/\tilde{\Lambda}$ in this bracket, are shown in Fig. 2 for a continuum film at $\tilde{\Lambda} = 4.243$. **FNGA** P profile departs from that of **INGA** mainly in its convex curvature in the land sub-domain; consequently $\bar{P} > 1$ and an entrance bias required by the ambient

boundary condition is $p_0 = p_a/\bar{P}$. **FNGA** Φ_c profile is not uniform in either sub-domain, being upwards inclined within a groove while downward inclined and convex in a film land. Test calculations for the 2-mm bearing show the influence of Kn_{aC} results in a very slight suppression of the large $\tilde{\Lambda}$ effects that are displayed in these profiles; they would be hardly distinguishable if superimposed in Fig. 2, hence omitted. It thus appears that **FNGA** can serve to bring out the significance of large $\tilde{\Lambda}$ in its simpler version for the continuum film until $Kn_a = O\{1\}$ becomes of interest. A parametric plot of $(\Lambda^{-1} P \partial P/\partial \zeta)_{\text{mean}}$ vs. Ψ can be named the pressurization line. A map of pressurization lines for $0 \leq \tilde{\Lambda} \leq 42.43$ (up to 1,000,000 RPM for the 2 mm bearing) is shown in Fig. 3. The **INGA** line is completely straight because its governing equation is linear with respect to $\Delta P/\tilde{\Lambda}$. Departure from the **INGA** line is very gradual, and can be regarded to be negligible up to $\tilde{\Lambda} = 4.243$ in spite of the distinguishing features in Fig. 2. It is quite remarkable that the line curvature is almost non-existent for $\tilde{\Lambda} = 42.43$ even though both vertical and horizontal intercepts are substantially reduced. The macro-scale solution is contained between the pressurization line for the prevailing ambient $\tilde{\Lambda}/\bar{P}$ and that of **INGA**.

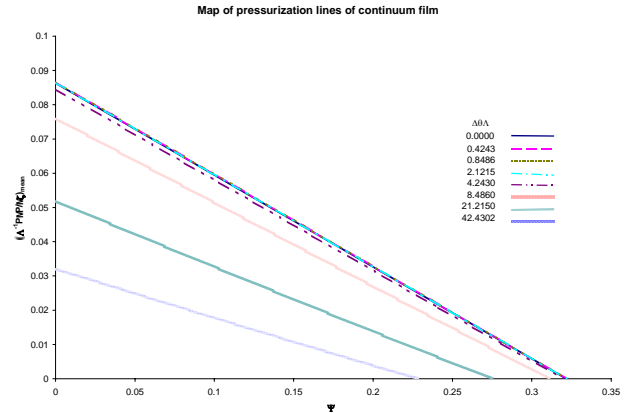


Fig. 3 Map of pressurization lines

REFERENCES

- [1] Whipple, R. T. P., 1951, "Theory of the Spiral Grooved Thrust Bearing with Liquid or Gas Lubricant," *Atomic Energy Research Establishment Technical Report No. 622*.
- [2] Bonneau, D., J. Huitric, and B. Tournerie, 1993, "Finite Element Analysis of Grooved Gas Thrust Bearings and Grooved Gas Face Seals," *ASME Journal of Tribology*, Vol. 115, pp. 348 - 354.
- [3] Zirkelback, N., and L. San Andrés, 1999, "Effect of Frequency Excitation on the Force Coefficients of Spiral Groove Thrust Bearings and Face Gas Seals," *ASME Journal of Tribology*, Vol. 121, 4, pp. 853-863.
- [4] Jang, G.H., K.S. Kim, H.S. Lee, and C.S. Kim, 2004, "Analysis of a Hydrodynamic Bearing of a HDD Spindle Motor at Elevated Temperature," *ASME Journal of Tribology*, Vol. 126, 2, pp. 353-359.
- [5] Kang, Soo-Choon, 1997, "A Kinetic Theory Description for Molecular Lubrication," Ph. D. Dissertation, Carnegie Mellon University. UMI Number 9801040.
- [6] Jäger, Diego A., 1987, "An Unconditionally Stable, High Resolution Algorithm for Gas Lubrication Problems," Dissertation in the School of Engineering and Applied Science, Columbia University. UMI order number 872404.